Mott insulator phases and first-order melting in $Bi_2Sr_2CaCu_2O_{8+\delta}$ crystals with periodic surface holes

S. Goldberg,[1] Y. Segev,[1] Y. Myasoedov,[1] I. Gutman,[1] N. Avraham,[1] M. Rappaport,[1] E. Zeldov,[1] T. Tamegai,[2] C. W. Hicks,[3] and K. A. Moler[3]

[1]*Department of Condensed Matter Physics, The Weizmann Institute of Science, Rehovot 76100, Israel*
[2]*Department of Applied Physics, The University of Tokyo, Hongo, Bunkyo-ku, Tokyo 113-8656, Japan*
[3]*Department of Physics and Geballe Laboratory for Advanced Materials, Stanford University, Stanford, California 94305, USA*

(Received 6 August 2008; revised manuscript received 23 January 2009; published 24 February 2009)

We measured the effects of periodic surface holes, created using a focused ion beam, on the phase diagram of the vortex matter in high-T_c $Bi_2Sr_2CaCu_2O_{8+\delta}$ crystals. Differential magneto-optical measurements show that the irreversibility line is shifted to higher fields and temperatures with respect to the pristine melting line. The irreversibility line displays weak field dependence between integer matching fields indicating multiple-flux-quanta pinning at holes. We find reduced equilibrium compressibility of the vortex matter at integer matching fields, which is strong evidence for the existence of thermodynamic Mott insulator phases. Shaking with a transverse ac field surprisingly reveals first-order melting that is not shifted with respect to the pristine melting line and that seems to occur within the Mott insulator regions. This melting is understood to be the first-order transition in the bulk of the crystal beneath the surface holes. The transition is visible at the surface, despite the reduced vortex compressibility in the top layer.

DOI: 10.1103/PhysRevB.79.064523 PACS number(s): 74.72.Hs, 74.25.Ha, 74.25.Bt

I. INTRODUCTION

Experimental and theoretical studies of high-T_c materials with correlated pinning centers have led to the discovery of many novel phases of vortex matter, nonexistent in the pristine materials. These new phases arise from the complex interplay among intrinsic point disorder, correlated disorder, vortex-vortex interaction, and temperature. Correlated disorder in high-T_c crystals is often introduced by heavy-ion irradiation along the crystallographic c axis, which leads to a random distribution in the a-b plane.[1,2] The effects of such random correlated disorder on the high-T_c phase diagram are relatively well understood, both theoretically[3–8] and experimentally.[9–12] Measurements of crystals with periodic correlated disorder are limited since it is not yet known how to physically realize periodic correlated disorder in thick samples. Experimental studies of periodic disorder must therefore choose between two options: study of thin samples or study of artificial pins located at the sample surface. Efforts have focused mainly on the study of thin superconducting films with periodic pinning centers.[13–23] However, thin films do not necessarily retain the thermodynamic properties of the bulk crystal due to enhanced point disorder. Comparison of the resulting vortex phases to the thermodynamic phases of the pristine material is thus usually not possible.

Theoretically, the thermodynamics of vortices in the presence of *random* correlated disorder have been studied extensively. Nelson and Vinokur[3] mapped the pinned vortex matter onto a system of quantum two-dimensional (2D) bosons. They predicted the Bose glass transition from the low-temperature Bose glass phase, in which vortices are localized, to a higher-temperature delocalized vortex phase. They also discussed the possibility of an incompressible Mott insulator (MI) phase when the magnetic induction of the sample B exactly equals the matching field $B_\phi=\rho\phi_0$, where ρ is the density of the columnar defects (CDs). Radzihovsky[5] extended this model to include additional phases for $B>B_\phi$: a low-temperature weak Bose glass phase, in which both vortices residing at pins and those at interstitial sites are localized, an interstitial liquid phase at intermediate temperature, in which interstitial vortices are free to move but those at pinning sites are still pinned, and a homogenous liquid phase at higher temperature, in which all vortices are delocalized. For *periodic* pinning centers, the various Bose glass phases may be modified.[24] For periodic surface holes, even such a modified description is expected to be valid only within some finite depth from the surface of the superconductor.

Simulations of two-dimensional systems containing periodic pinning centers that allow only single-vortex occupancy demonstrate commensurate states at integer matching fields nB_ϕ, with permitted values of n depending on the geometry of the pinning centers.[25] Solutions of Ginzburg-Landau theory reveal additional commensurate states with multiquanta vortices[26,27] for more general sample and pinning center parameters. Different melting scenarios have been demonstrated for triangular and kagome arrays at low matching fields[28] and for square pinning arrays both at and in between matching fields.[29] The square pinning array at the first matching field displays three phases: a low-temperature pinned solid with square geometry, an unpinned ("floating") solid with triangular geometry, and a high-temperature liquid that lacks long-range order. At higher commensurate matching fields, the floating solid phase is not found, but an intermediate phase with mobile interstitial vortices similar to the liquid is observed. Incommensurate fields display a pinned phase at low temperatures with extra vortices located at interstitial positions, a phase at intermediate temperatures in which some vortex motion is present with both interstitials and pinned vortices participating, and a phase at higher temperatures, in which all vortices are mobile. The temperature at which mobility is observed for incommensurate fields is lower than the melting temperature at the commensurate matching fields.[29] For the triangular and kagome geometries, melting at the first matching field involves a low-temperature pinned solid and a high-temperature liquid only. Intermediate-temperature phases, in which some or all of the interstitial vortices are mobile, are observed at higher matching fields.[28] These melting transitions are expected to be most relevant to high-T_c superconductors.[29]

Direct imaging experiments of low-T_c thin films with artificial periodic disorder have shown that highly ordered vortex states exist at integer nB_ϕ and fractional $(p/q)B_\phi$ matching fields, with n, q, and p integers.[30,31] Due to these ordered vortex states, such films have demonstrated commensurate effects in critical current,[13–16] magnetization,[17] magnetoresistance,[18,19] and magnetic-susceptibility measurements.[20–23] Possible phases and phase transitions of the vortex matter have been inferred from these measurements. Enhanced flux creep rate for $B>B_\phi$ was thought to be evidence of a transition from an incompressible MI state to an interstitial liquid state.[17] Shapiro steps in transport measurements were understood to be a result of the coexistence of vortices pinned to artificial pinning sites and mobile interstitial vortices.[32] The behavior of the critical current was interpreted as evidence of two depinning energies, corresponding to the upper boundaries of the weak Bose glass and interstitial liquid phases.[19] Onsets of nonzero real and imaginary parts of the magnetic susceptibility were tentatively identified as the lower and upper phase boundaries of an interstitial liquid phase.[22] In addition to these states, the possibility of a saturation number $n_s>1$, corresponding to n_s vortices at each pinning site, leads to multiple-quanta pinned vortex states, which have been observed in many samples.[15,23]

There are fewer experimental data regarding the thermodynamic phases of high-T_c superconductors with periodic artificial pinning centers. The critical current in $YBa_2Cu_3O_7$ (YBCO) thin films exhibited integer commensurate effects[33] over a large temperature range. Scanning Hall probe measurements indicated that trapping of $\sim$15 flux quanta is possible for 2.5-μm-diameter holes close to T_c in YBCO.[34] Thin crystalline $Bi_2Sr_2CaCu_2O_{8+\delta}$ (BSCCO) samples with fully penetrating periodic holes exhibited integer[35] and rational[36] matching effects, in magnetoresistance and transport measurements, respectively. Similar samples with surface holes also displayed matching effects in magnetoresistance and critical current.[37] A single study using thick BSCCO samples with surface holes displayed integer matching in local magnetization.[38] In these studies of BSCCO, the matching effects were visible in the field and temperature ranges at which the vortex matter is known to be in a liquid state in pristine crystals. No first-order melting step[39] was measured in these samples, and a full description of thermodynamic phases and transitions is lacking.

In this work, we present an investigation of a thick BSCCO crystal, partially patterned with periodic surface holes created by a focused ion beam, measured using differential magneto-optics (DMO) (Refs. 40–42) accompanied by shaking with transverse ac field.[43] We observe steplike behavior of the irreversibility line (IL), which may be a result of multiquanta pinning to holes. We see a reduction in the DMO signal at integer matching fields, evidence of MI phases. We find a first-order melting transition (FOT) in the patterned regions that is not shifted with respect to the pristine melting line. This FOT is observed even at integer matching fields, where the vortex matter in the surface layer is essentially incompressible. We believe this FOT to be the melting transition of the bulk of the crystal beneath the patterned surface.

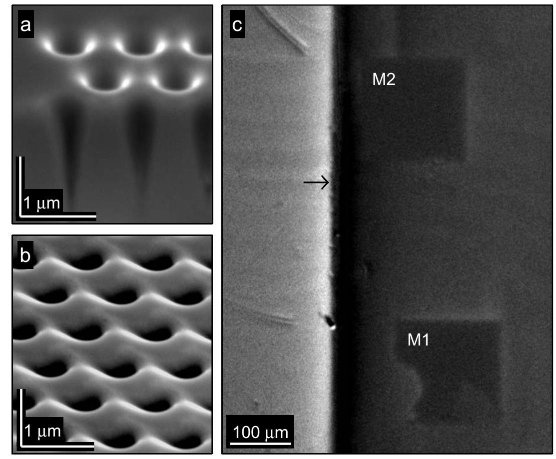

FIG. 1. (a) Scanning electron microscopy (SEM) image of the cross section of the surface holes. Hole depth is $\sim$1.4 μm. (b) Part of one of the two arrays patterned on the sample, imaged by SEM. The distance between holes is 0.9 μm. (c) A DMO image of the sample at T=80 K and H=21 Oe. The sample's edge is the vertical border indicated by the arrow. The two B_ϕ=29.5 G arrays, M1 and M2 of 170$\times$170 μm^2, appear as darker regions due to their enhanced irreversibility. The irregular shape of M1 is a result of surface damage that occurred after writing the holes.

II. EXPERIMENTAL DETAILS

Several samples were prepared and studied. Here we present a detailed investigation of a 2750$\times$740$\times$30 μm^3 BSCCO crystal ($T_c\simeq$90.5 K), with two triangular arrays of periodic holes patterned on the top surface using an FEI Strata 400 focused ion-beam system. Figures 1(a) and 1(b) show SEM images of the hole profile and periodicity, respectively. The measured hole depth was approximately 1.4 μm. Hole diameter decreases from $\sim$0.6 μm at the sample surface to $\sim$0.3 μm at a depth of 0.7 μm. The lattice constant of both arrays was 0.9 μm, corresponding to a matching field of B_ϕ=29.5 G. The dimensions of each array were approximately 170$\times$170 μm^2.

DMO measurements were performed by modulating the applied field $H\parallel c$ axis by ΔH=1 Oe while sweeping temperature T at constant H or scanning H at constant T. Each measurement point required averaging over k charge-coupled device (CCD) camera exposures, first at $H+\Delta H/2$ and then at $H-\Delta H/2$, and calculating a difference image. Each DMO image is the average of m such difference images. Using $k,m\sim 10$ with a typical exposure time of 0.3 s yielded a typical modulation frequency of $\sim$0.33 Hz. Values of dB/dH were derived from the DMO images by dividing the local light intensity by the intensity of some region far from the sample, where it was assumed that $dB/dH=1$ G/Oe. For quantitative data analysis, intensities were spatially averaged over a typical area of $\sim 50\times 50$ μm^2. As described previously,[40–42] the DMO measurement with field modulation is essentially equivalent to the measurement of the real component of the low-frequency local ac susceptibility as obtained, e.g., by Hall sensors.[44] Figure 1(c) shows a DMO image of part of the sample taken at $T=80$ K and $H=21$ Oe. The average brightness of the patterned areas M1 and M2 is lower than that of the neighboring pristine sample. This is due to an elevated IL in the patterned areas as described below.

III. RESULTS

We first inspect the IL of the patterned regions. The IL is important in the context of possible Bose glass phases because it is thought to be the dynamic manifestation of the thermodynamic Bose glass transition.[3] In DMO measurements, reversibility of the vortex matter is quantified by modulating the applied field by ΔH and measuring dB/dH, the change in the local magnetic induction due to the modulation. Strong pinning results in $dB/dH=0$, whereas full reversibility corresponds to $dB/dH=1$ G/Oe. The irreversibility threshold in the following was chosen arbitrarily at $dB/dH=0.8$ G/Oe, with $T_{\mathrm{IL}}(H_{\mathrm{IL}})$ denoting the temperature (external field) at which this threshold is reached. We emphasize that the resulting IL reflects the response of the vortex system at low frequencies. Transport measurements or DMO with current modulation could possibly map out additional boundary lines similar to the delocalization line of vortices from columnar defects;[12] however, such measurements are beyond the scope of the present study. Figure 2 shows dB/dH for the pristine region [Fig. 2(a)] and patterned region M1 [Figs. 2(b) and 2(c)] measured by T scans at constant H.

Focusing on the pristine region [Fig. 2(a)], we see a series of sharp peaks in dB/dH with paramagnetic $dB/dH>1$ (light gray, light pink online), corresponding to the first-order melting transition T_m from a low-temperature vortex solid to a high-temperature vortex liquid.[40,45] The black dots in Fig. 2(b) show the pristine melting line T_m extracted from Fig. 2(a). The patterned region M1 [Fig. 2(b)], in comparison, shows no FOT. It does, however, exhibit two notable features. First, the IL of region M1 is shifted to higher temperature. This is seen by focusing on T_{IL} (white contour) in Figs. 2(a) and 2(b). T_{IL} of the patterned region M1 is significantly greater than T_{IL} of the pristine region, which occurs at temperatures lower than the pristine T_m. The second notable feature in Fig. 2(b) is a narrow finger near $H=33$ Oe, approximately 1 Oe wide, for $82<T<87$ K, in which dB/dH of M1 is suppressed.

Figure 2(c) shows dB/dH of patterned region M1 over a larger range of H and T. The pristine melting line T_m is plotted as black dots for comparison. The IL of M1 is clearly shifted to higher temperatures. Sharp fingers, or narrow regions of H in which dB/dH of M1 is highly suppressed, occur at $H=33$, 64, 95, 126, and 157 Oe (denoted by arrows), consistent with integer multiples $B/B_{\phi}=1$, 2, 3, 4, and 5 of the predicted matching field $B_{\phi}=29.5$ G. The minima in dB/dH as a function of H at matching fields are of both dynamic and thermodynamic origin. Enhanced pinning at matching fields suppresses vortex motion, and hence also dB/dH. As discussed below, these minima also indicate narrow ranges of H with reduced equilibrium compressibility since the compressional modulus c_{11} is proportional to dH/dB.[46] In addition to the fingers observed *at* integer B/B_{ϕ}, we see that T_{IL} *between* matching fields is steplike, with $T_{\mathrm{IL}}(H)$ weakly dependent on H between matching fields, and shifts in $T_{\mathrm{IL}}(H)$ occurring at matching fields. For example, $T_{\mathrm{IL}}\approx 76.5$ K for $3<H/B_{\phi}<4$ and $T_{\mathrm{IL}}\approx 74$ K for $4<H/B_{\phi}<5$ (white contour).

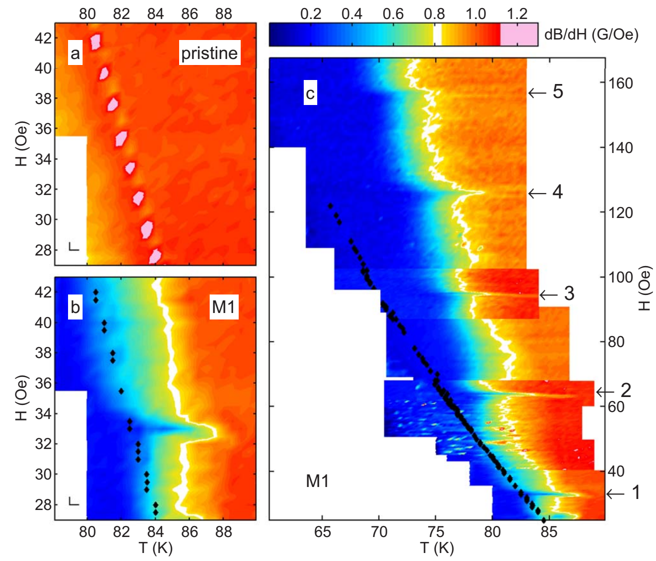

FIG. 2. (Color online) dB/dH, the change in magnetic induction due to field modulation of $\Delta H=1$ Oe, for different sample regions, taken during T scans. (a) A pristine region. The pristine melting line T_m appears as a series of light gray (light pink) paramagnetic peaks in dB/dH with values above 1 G/Oe. This particular run was carried out on a sparse grid in T and H of 0.4 K and 0.5 Oe (denoted by the lines in the lower left corner). The apparent discontinuity in T_m is an artifact resulting from grid spacing larger than the width of the melting peak. (b) dB/dH of region M1 in the vicinity of the first matching field, $B_{\phi}=29.5$ G. dB/dH values are reduced compared to (a) and a narrow dip appears at $H=33$ Oe. The location of the pristine melting line T_m is denoted by black points. (c) dB/dH in the patterned region M1 over a wide range of T and H. Matching effects (denoted by arrows) are visible at $H=33$, 64, 95, 126, and 157 Oe, consistent with integer multiples of the predicted $B_{\phi}=29.5$ G. The pristine melting line T_m is denoted by black points. The patches in the data are a result of slightly differing setup parameters for the different experimental runs.

We now focus on the IL of the patterned regions below and in the vicinity of the first matching field. Figure 3 shows dB/dH measured simultaneously in the pristine region and in the patterned regions M1 and M2 for $B\lesssim B_{\phi}$. T_{IL} ($dB/dH=0.8$ G/Oe, white contour) of the pristine region is located below the pristine melting line T_m. In region M1 [Fig. 3(b)], T_{IL} is shifted to higher temperatures at all fields when compared to the T_{IL} of the pristine region [Fig. 3(a)]. An addi-

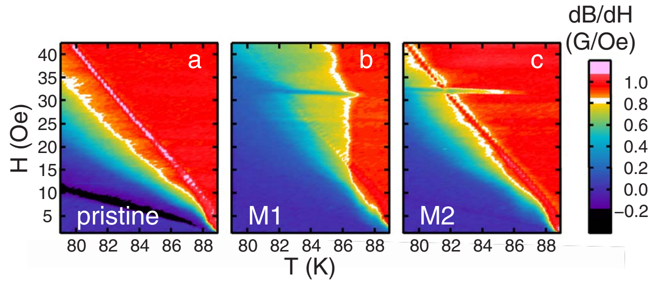

FIG. 3. (Color online) dB/dH for $B \lesssim B_\phi$, measured during T scans. (a) dB/dH of a pristine region. The melting transition T_m appears as a line with $dB/dH > 1$ G/Oe (light gray, light pink online). The temperature T_{IL} at which the IL is located ($dB/dH = 0.8$ G/Oe, white) is found below T_m. (b) and (c) show dB/dH of patterned regions M1 and M2, respectively. T_{IL} of M1 and M2 is shifted to higher temperatures relative to the pristine T_{IL}. A sharp finger in T_{IL} of both M1 and M2 appears at $H = 33$ Oe, where $B = B_\phi$. Negative values of dB/dH (black) correspond to negative permeability due to geometrical barriers.

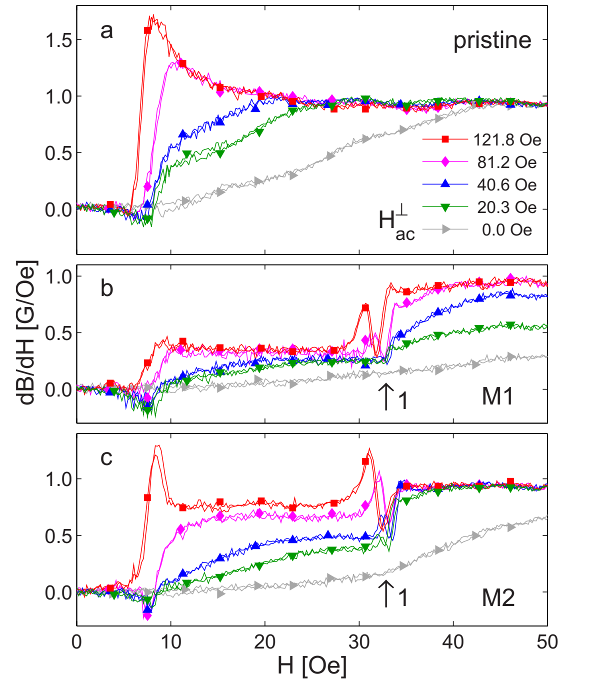

FIG. 4. (Color online) dB/dH vs applied field H (scanned up and down) for different values of in-plane shaking amplitude $H_{\mathrm{ac}}^{\perp}$ at $T = 77$ K for the (a) pristine region and patterned regions (b) M1 and (c) M2. Arrows denote the first matching field. Data are shown for different values of applied $H_{\mathrm{ac}}^{\perp}$ (from bottom to top): 0 (▷), 20.3 (▽), 40.6 (△), 81.2 (◇), and 121.8 (□) Oe. Shaking frequency was 15 Hz for all measurements. Symbols appear every 37 data points.

tional sharp finger in the IL, extending to $T_{\mathrm{IL}} \simeq 87$ K, occurs at $H = 33$ Oe or $B = B_\phi$. The IL of patterned region M2 [Fig. 3(c)] is shifted somewhat less, yet it too displays a sharp shift to higher T at the matching field B_ϕ. The reason for the difference in the shift of the IL of the two arrays may be a result of the difference in the arrays' locations (M2 is closer to the sample's edge) or due to some difference in the holes of the two arrays, which are not identical and may have different pinning properties. Still, for both arrays the IL is shifted upward, with an additional sharp finger at B_ϕ. In BSCCO crystals irradiated with low concentration of CDs the sharp finger is absent. Instead, a kink is observed in the vicinity of B_ϕ which is believed to be the result of depinning of two different vortex populations. Below B_ϕ, T_{IL} is the temperature at which vortices located at CDs depin. Above B_ϕ, T_{IL} is the depinning temperature of interstitial vortices.[12] Also, fractional matching features have been observed[37] in BSCCO samples with periodic surface defects. We do not detect any fractional matching features in the IL of the patterned regions; the reason for this is not clear but is consistent with results shown elsewhere.[38]

The IL in BSCCO is known to be a dynamic feature of the phase diagram.[4,47,48] However, since it indicates a region of the phase diagram in which there is a change in the system's dynamic response, it may indicate an underlying thermodynamic transition that occurs at similar values of field and temperature. In order to detect a possible underlying FOT, and to determine whether the reduced dB/dH regions are truly a thermodynamic feature of the phase diagram, we studied the behavior of the first matching field in the presence of shaking. The shaking technique[43] utilizes an in-plane ac magnetic field. It is known to suppress hysteretic behavior in BSCCO, enabling the observation of thermodynamic properties.[48–50]

The effect of shaking is shown in Fig. 4 for the pristine and patterned regions M1 and M2 at 77 K. Increasing shaking amplitude $H_{\mathrm{ac}}^{\perp}$ leads to a systematic increase in dB/dH, which saturates near 1 G/Oe, as expected for a fully penetrable sample. A feature common to all three plots in Fig. 4, and thus unrelated to the surface holes, is an abrupt change from zero to negative dB/dH at $\simeq 8$ Oe. Below $\simeq 8$ Oe, the sample is in the Meissner phase, with $B = 0$. $dB/dH < 0$ immediately above the Meissner phase corresponds to negative local permeability.[51] This effect, which occurs in BSCCO samples with platelet geometry, is a result of the geometrical barrier[52,53] and the modulation of the vortex dome during the modulation cycle of the applied field $H \pm \Delta H/2$. This negative permeability is also visible as a black strip at low fields in Fig. 3(a). It is interesting to note that the negative dB/dH values are not visible at the highest shaking amplitude $H_{\mathrm{ac}}^{\perp} = 121.8$ Oe. This indicates that the shaking field enables the vortices to overcome the geometrical barrier. Consequently, the local negative permeability changes to high positive local permeability, as seen in Figs. 4(a) and 4(c). This is the expected behavior in the absence of geometrical barriers, as demonstrated for prism-shaped samples.[54]

There are two notable differences between the pristine [Fig. 4(a)] and patterned [Figs. 4(b) and 4(c)] regions. The first difference is the appearance of the matching feature in the form of a dip in dB/dH near 32 Oe, denoted by arrows in Fig. 4. Shaking extends the range of temperatures for which this dip is visible well into the vortex solid region below T_m. Without shaking, the first matching feature is not visible at this temperature (77 K, see Fig. 2) due to the enhanced pinning in the vortex solid. With increased $H_{\mathrm{ac}}^{\perp}$, the matching feature appears first as a step [Fig. 4(b), $H_{\mathrm{ac}}^{\perp} = 20.3$ and 40.6 Oe] and then as a dip in dB/dH ($H_{\mathrm{ac}}^{\perp} = 81.2$ Oe). In some cases, as shown in Fig. 4(c) for high $H_{\mathrm{ac}}^{\perp}$, a peak appears in

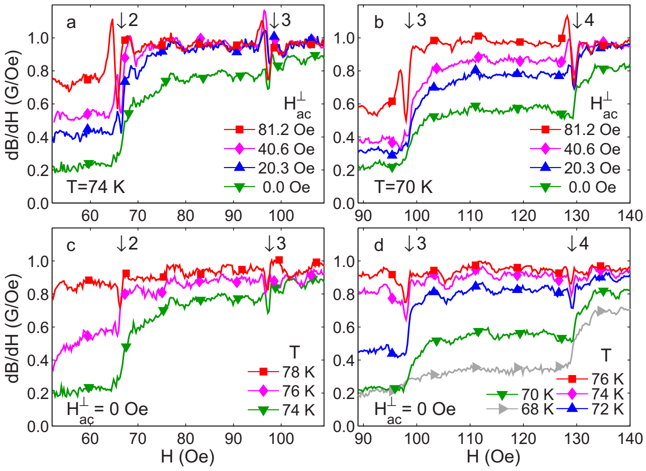

FIG. 5. (Color online) dB/dH of region M2 as a function of H for different temperatures T and shaking amplitudes $H^{\perp}_{ac}$. The effect of shaking is similar to the effect of temperature (see text). (a) Matching effects at $T=74$ K and $B/B_{\phi}=2$ and 3 and (b) at $T=70$ K and $B/B_{\phi}=3$ and 4. $H^{\perp}_{ac}=0$ (▽), 20.3 (△), 40.6 (◇), and 81.2 (□) Oe. (c) Matching effects at $T=74$ (△), 76 (◇), and 78 (□) K; $B/B_{\phi}=2$ and 3, without shaking. (d) Matching effects at $T=68$ (▷), 70 (▽), 72 (△), 74 (◇), and 76 (□) K; $B/B_{\phi}=3$ and 4, without shaking. Arrows denote matching fields. Symbols appear every 30 data points.

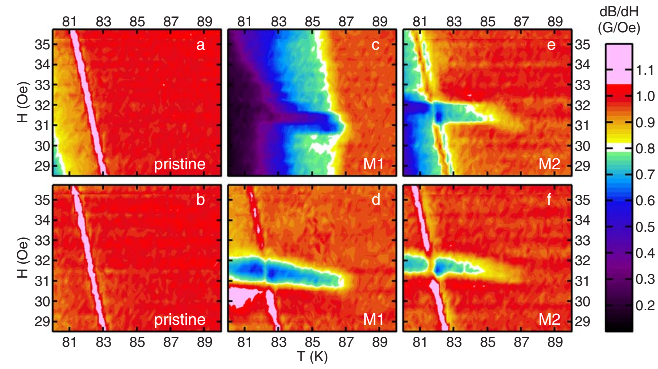

FIG. 6. (Color online) dB/dH as a function of H and T near the intersection of melting and $B/B_{\phi}=1$ matching, without (top panels) and with (bottom panels) shaking. Shaking parameters were 15 Hz and 81.2 Oe. Results are shown for the [(a) and (b)] pristine sample and patterned regions M1 and M2 [(c) and (d) and (e) and (f), respectively].

dB/dH immediately before the dip. The slight downward shift in H of the dip for increasing $H^{\perp}_{ac}$ probably results from the increased penetration of magnetic induction B at higher $H^{\perp}_{ac}$, resulting in the same $B=B_{\phi}$ at slightly lower values of applied field H. The dip in dB/dH corresponds to a reduction in the compressibility of the vortex matter at B_{ϕ}.

The second difference between the pristine and patterned regions in Fig. 4 can be seen away from the matching field. For the pristine region, the values of dB/dH increase gradually from $dB/dH\simeq 0$ at low field to $dB/dH=1$ G/Oe at sufficiently high applied field H. For the patterned regions, the behavior of dB/dH is plateaulike, with the matching feature dividing between neighboring plateaus. This can be seen in Fig. 4(b) for $H^{\perp}_{ac}=81.2$ and 121.8 Oe and in Fig. 4(c) for $H^{\perp}_{ac}=40.6$ Oe. These plateaus are consistent with the observed steplike behavior of T_{IL} during T scans, as shown in Fig. 2(c). The plateaus in dB/dH appear between matching fields, where T_{IL} is almost independent of H. The step between the plateaus appears at $H=B_{\phi}$, consistent with the steps in T_{IL} that occur at $H=nB_{\phi}$. The value of dB/dH for each plateau in Figs. 4(b) and 4(c) increases with increasing $H^{\perp}_{ac}$. Figures 5(a) and 5(b) show the effects of shaking with different values of $H^{\perp}_{ac}$ for $B/B_{\phi}=2$ and 3 and $B/B_{\phi}=3$ and 4, respectively, for patterned region M2. The data for M1 are similar. Clearly the same matching features that appear for $B/B_{\phi}=1$, namely, a step in dB/dH for low $H^{\perp}_{ac}$ that develops into a dip for higher $H^{\perp}_{ac}$ are visible also for higher matching fields.

Interestingly, increasing T and increasing shaking amplitude $H^{\perp}_{ac}$ have similar effects on dB/dH immediately below the IL. This can be seen by comparing Figs. 5(a) and 5(c), in which dB/dH of region M2 in the vicinity of $B/B_{\phi}=2$ and 3 is plotted for different values of $H^{\perp}_{ac}$ and T, respectively. Increasing $H^{\perp}_{ac}$ and increasing T (from bottom to top curves) both tend to increase dB/dH and both have the effect of transforming the matching feature from a step to a dip. However, the overshoot in dB/dH immediately below the matching feature appears only at nonzero $H^{\perp}_{ac}$. Similar behavior is observed for $B/B_{\phi}=3$ and 4 in Figs. 5(b) and 5(d).

We now address the question of first-order melting within the patterned regions in the presence of shaking. For the results shown below, we applied 15 Hz $H^{\perp}_{ac}=81.2$ Oe shaking field. We find that shaking shifts the IL to lower fields and temperatures and thus enables the observation of a FOT in the patterned regions of the sample. Figure 6 shows detailed scans of the H-T region in which the pristine T_m line intersects the $B/B_{\phi}=1$ matching line. dB/dH is shown for both patterned regions and for the pristine region, without and with shaking (top and bottom panels, respectively). For the pristine region [Figs. 6(a) and 6(b)], dB/dH at lower T and H is raised slightly by shaking and the pristine melting line T_m, which appears as a line with paramagnetic $dB/dH > 1$ G/Oe (light gray, light pink online), remains essentially unchanged. For the patterned region M1, no FOT was visible without shaking [Fig. 6(c)]. With shaking [Fig. 6(d)], a FOT became visible. It appears to be located at the same temperatures and fields as the pristine melting line T_m. Remarkably, the T_m line is clearly visible even at the bottom of the B_{ϕ} matching dip. For the patterned region M2, shaking was not needed to uncover the FOT [Fig. 6(e)]. While shaking raised dB/dH values overall, it did not change the location or the nature of the FOT [Fig. 6(f)]. Similar results are shown for $B/B_{\phi}=2$ in Fig. 7. In this case, shaking was necessary to view the FOT in both patterned regions M1 [Figs. 7(c) and 7(d)] and M2 [Figs. 7(e) and 7(f)]. Note that the location of the FOT of the patterned regions in the phase diagram is indistinguishable from the location of the pristine melting line T_m. Moreover, T_m and the nB_{ϕ} lines seem to intersect with no apparent interaction, as if the periodic pinning potential of the holes has no effect on melting. No additional FOT was detected for either of the patterned regions. We emphasize that at the points in the phase diagram where the FOT meets the matching fields, a contradictory behavior of

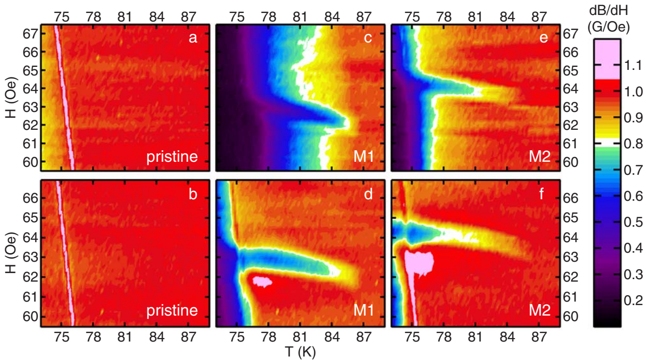

FIG. 7. (Color online) dB/dH as a function of H and T near the intersection of melting and $B/B_\phi=2$ matching, without (top panels) and with (bottom panels) shaking. Shaking parameters were 15 Hz and 81.2 Oe. Results are shown for the [(a) and (b)] pristine sample and patterned regions M1 and M2 [(c) and (d) and (e) and (f), respectively]. The slight curving of the matching effect to lower H for higher T in (c)–(f) is due to the increased penetration $B(H)$ at higher T.

the vortex lattice occurs. On one hand, at the FOT there is a *jump in vortex density*. On the other hand, at matching fields the vortex matter exhibits a *strongly enhanced compressibility modulus* $c_{11}\sim(dB/dH)^{-1}$ that exists both below and above T_m. This apparent contradiction is discussed below.

IV. DISCUSSION

In order to understand the observed behavior of the IL, we consider two possible physical scenarios.[55] In the first scenario, shown schematically in Fig. 8(a), we assume that each hole can pin only a single vortex. As a result, two vortex populations are present for $B>B_\phi$: vortices located at holes and interstitial vortices located between holes. The interstitial vortices are subjected to a caging potential caused by the vortices located at holes[24] that is assumed to be weaker than the pinning potential at holes but stronger than the pristine pinning. This gives rise to a depinning transition of the interstitials, which we identify with T_{IL}, at a temperature above the pristine melting temperature T_m. Alternatively, we consider a scenario in which there is a multiquanta pinning by holes. We assume that below the IL, all vortices are located at holes, while above the IL, some vortices are depinned from holes, and thus mobile, as shown schematically in Fig. 8(b). Due to repulsion between pinned vortices, the pinning force per vortex is expected to decrease as a function of the number of vortices pinned to the hole.[56] We therefore assume that the pinned vortices residing at holes depin one at a time, as T is increased. Within this multiquanta scenario, T_{IL} corresponds to the temperature at which the first vortices depin from holes. Either of the two scenarios must provide an explanation for the observed behavior of the IL: the plateaus in the IL *away from* matching, the shift in the IL to lower T and H in the presence of shaking, and the sharp dips at the matching fields.

We begin with the plateaus and steps in the IL. In the multiquanta scenario, the maximum number of vortices per hole $n_{\max}(T)$ is determined by temperature-dependent hole

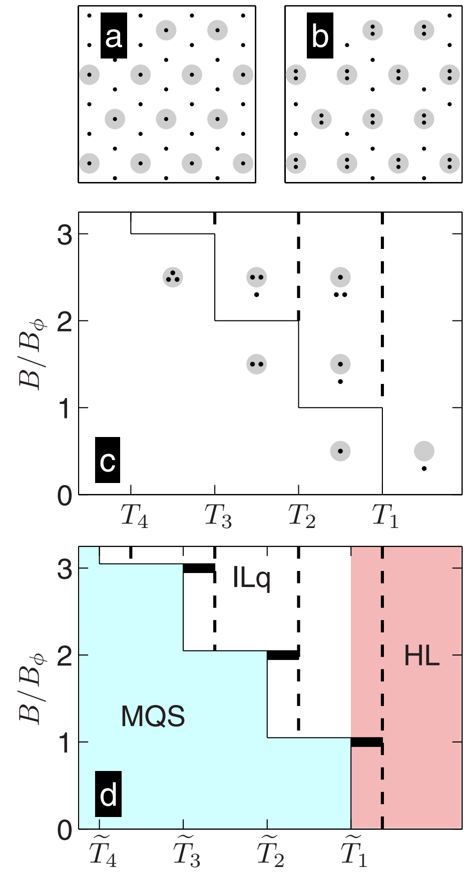

FIG. 8. (Color online) (a) and (b) A schematic view of the vortex matter for $B/B_\phi=3$, within (a) the single-vortex pinning scenario and (b) the multiquanta scenario. Gray circles indicate holes. Black dots indicate vortices. (a) In each unit cell of the pinning lattice, a single vortex is pinned to the hole and two vortices are interstitial. Below (above) the IL interstitials are pinned (mobile). (b) In each unit cell, two vortices remain pinned to the hole. Below the IL the third vortex is also pinned to the hole (not shown). Above the IL, it is depinned and mobile. (c) and (d) A schematic description of the steps in the IL, within the multiquanta scenario, in the (c) absence and (d) presence of thermal fluctuations or shaking. (c) The maximum number of quanta per hole $n_{\max}(T)$ (solid black line) is expected to decrease as a function of T, resulting in temperatures T_n (dashed lines) above which holes pin $n-1$ vortices only, and additional vortices become mobile interstitials. Thus for each interval $(n-1)<B/B_\phi<n$, $T_{\text{IL}}=T_n$. (d) Thermal fluctuations shift T_{IL} (solid line) from T_n (dashed lines) to $\tilde{T}_n<T_n$. At $B/B_\phi=n$, the vortex lattice remains stable to the temperature T_n due to a thermodynamic MI phase. Resulting phases include a multiquanta solid (MQS) below T_{IL}, an interstitial liquid (ILq, white) above the IL that terminates at $\tilde{T}_1$, a homogeneous liquid (HL) above $\tilde{T}_1$, and MI fingers at $B/B_\phi=n$ (black).

pinning strength and repulsive interactions between vortices located at the hole and decreases with increasing temperature.[56] We denote the temperature at which $n_{\max}$ decreases from n to $n-1$ by T_n [see dotted lines in Fig. 8(c)]. We assume that for the applied fields $H\leq 6B_\phi$, all vortices are pinned to holes at sufficiently low T. As T is increased above T_n, holes may only pin $n-1$ vortices. Therefore vortices abruptly depin from holes occupied by n vortices, leaving $n-1$ vortices per hole. The depinned vortices are mobile, leading to a fast onset of reversibility. We therefore identify $T_{\mathrm{IL}}=T_n$ for $(n-1)<B/B_\phi<n$. The resulting IL thus displays steps and plateaus, as shown schematically in Fig. 8(c). Finite temperature and slight hole variability are likely to cause some variation in $n_{\max}(T)$ at different holes. This would lead to some smearing of the irreversibility transition and to a weak dependence of T_{IL} on B between matching fields due to different mixing of the T_n as field is varied. This schematic description neglects the effects of thermal fluctuations, which will be discussed later on. The IL shown in Fig. 2(c) (white contour) indicates that T_{IL} displays three discrete steps in the temperature range $T=72-77$ K. The weak temperature dependence of the IL between matching fields, as well as the plateaus in dB/dH in Figs. 4 and 5, seems to indicate that the IL is not strongly affected by interactions between vortices at neighboring holes. Rather, it is governed by the hole pinning energy and the repulsion between vortices within a single hole, leading to the steplike T_{IL}. Within the single-vortex pinning scenario, in contrast, $T_{\mathrm{IL}}(H)$ is the depinning temperature of interstitial vortices that is expected to decrease rather smoothly with field as the density of interstitials increases.

We now address the shift of the IL to lower temperatures in the presence of shaking. Shaking and increased thermal fluctuations seem to have a similar effect on the IL (see Fig. 5). Within the multiquanta scenario both provide a mechanism for hopping of vortices between vacancies at holes, thus increasing the dynamic dB/dH and decreasing T_{IL}. Between matching fields and slightly below T_{IL}, the holes are below their full pinning capacity, so shaking may provide a way for vortices to hop between holes more easily or to depin from holes and move to interstitial positions. The plateaulike behavior indicates that this shaking-induced hopping is roughly independent of the number of vacancies that exists. Instead, the degree of hopping or depinning is dependent on the balance between the roughly field-independent pinning energy of the $n_{\max}$th vortex and the activation energy of the applied shaking. Within the single-vortex pinning scenario, above the IL the interstitials are mobile; therefore, immediately below the IL they are weakly pinned. Shaking will thus assist in overcoming the weak pinning potential, decreasing T_{IL}. The existence of the plateaus, however, cannot be easily explained in this case.

We now address the third experimental finding, namely, the fingerlike dips in dB/dH at matching fields. Focusing on Figs. 6 and 7, we see that, unlike the rest of the IL, the temperatures at which the fingers terminate are *not* affected by in-plane shaking. This strongly suggests that unlike the IL, which is a *dynamic* feature of the phase diagram, the fingers at matching fields are a *thermodynamic* feature. A thermodynamic minimum with $dB/dH=0$ would indicate a plateau in the equilibrium $B(H)$ and a diverging bulk modulus $c_{11}\sim\partial H/\partial B$,[46] which are clear signatures of the incompressible MI phase. The finite positive minima observed in dB/dH [see Figs. 4(b), 4(c), and 5] correspond to a reduction in the positive slope of $B(H)$ at nB_ϕ. These finite values at nB_ϕ may be a consequence of the finite size of the patterned region, which prevents infinite divergence of c_{11}, or of the broadening of dB/dH due to the modulation of $\Delta H=1$ Oe, which is at least as wide as the width of the dip. For samples with random defects, it has been argued that the MI phase is destroyed by repulsive vortex interactions, possibly retaining "lock-in" effects such as a finite peak in the bulk modulus c_{11}.[46,57] In our measurements, however, the pinning is ordered. At matching fields, pinning energy and vortex-vortex interactions both stabilize the vortex lattice. In this case, observation of a MI phase is possible.[46,57] We believe that the sharp matching features we observed in dB/dH at nB_ϕ that are not affected by shaking are a strong indication of thermodynamic MI phases.

The fingers of reduced dB/dH, or MI phases, may be understood in the context of the multiquanta scenario. For $(n-1)<B/B_\phi<n$ and $T<T_n$, in the absence of thermal fluctuations, all vortices are pinned to holes [see Fig. 8(c)]. The maximum number of vortices that can be pinned nB_ϕ/ϕ_0 is greater than the actual number of vortices B/ϕ_0, resulting in below-full occupancy, or "vacancies," at some of the multiquanta holes. Thermal fluctuations [which were neglected in the schematic description in Fig. 8(c)] are expected to lead to vortex hopping between the vacancies, resulting in enhanced vortex mobility. Thus, for $(n-1)<B/B_\phi<n$, vortex dynamics lead to a reduction in T_{IL} from T_n [Fig. 8(d), dashed lines] to some lower temperature $\tilde{T}_n$. Exactly at matching, an additional thermodynamic consideration enters. The total hole capacity equals the number of vortices, and therefore there is a finite energy cost for adding an extra interstitial vortex. As a result, the equilibrium $B(H)$ will exhibit a plateau over a finite range of H that is not affected by shaking. The corresponding minima in dB/dH, or equilibrium MI phases, may thus be observed up to T_n [black fingers in Fig. 8(d)].

The fingers of reduced dB/dH may also be partially understood within the single-vortex pinning scenario. At matching fields, we expect both the vortices at holes and the interstitials to be ordered in a configuration commensurate with the hole array that enhances the pinning potential and may result in a thermodynamic MI phase. Although this picture is correct for commensurate matching fields ($B/B_\phi=1,3,4,7,\ldots$, for a triangular array of holes[25]), it is not strictly correct for incommensurate matching fields. At $B/B_\phi=2$, for example, there are two interstitial positions with equal energy per unit cell. This would imply that hopping of interstitials is possible also at incommensurate matching fields, resulting in greater interstitial mobility, and hence a weaker matching effect. This is not what we observe in Fig. 2(c), where the fingers appear similar at the first and second matching fields.

We now consider the theoretical plausibility of the multiquanta scenario. The condition given for multiple-quanta pinning in holes is[58] $r^3>\xi\lambda^2$ for $\lambda\ll d$, where r is the hole radius, d is the interhole distance, and $\lambda=\lambda_0/\sqrt{1-T/T_c}$ is the London penetration depth.[4] For $r=0.2$ μm and $\lambda_0=0.15$ μm,[59] we may expect multiple-quanta vortices for $T\leq 88$ K for our sample.

We now estimate the number of vortices pinned at a hole as a function of temperature. We consider two physical possibilities, following Ref. 56. The first is that the nth vortex is pinned as long as there is some force near the edge of the hole that pushes it inward. This corresponds to a pinned state that may be metastable, depending on its free energy. The saturation number

$$n_s \approx r/2\xi \tag{1}$$

is the maximum n for which this occurs. The second possibility for multiple-quanta pinning is to require an equilibrium pinned state, namely, the free energy of the nth vortex located in the hole must be lower than its free energy far from the hole. In this case, the number of pinned vortices is given by[56]

$$n_0 \approx \frac{1}{2}\ln\frac{r}{2\xi} \bigg/ \ln\frac{2\lambda}{1.78r}. \tag{2}$$

Both n_s and n_0 decrease with T, which is consistent with the observed downward steps in $H_{\mathrm{IL}}(T)$. Substituting $r = 0.2\ \mu\mathrm{m}$, $\xi_0 = 2\ \mathrm{nm}$, $\lambda_0 = 0.15\ \mu\mathrm{m}$, and $T_c = 90.5\ \mathrm{K}$, we obtain $n_s = 1-21$ for $T = 90.46\ \mathrm{K}$ down to $T = 74.5\ \mathrm{K}$ and $n_0 = 1-2$ for $T = 85.2\ \mathrm{K}$ down to $T = 76.1\ \mathrm{K}$. Note that Eq. (2) was derived from the pinning energy of a *single* hole. In the case of an *array* of holes, one should compare the free energy of a pinned nth vortex to its free energy at the midpoint between two neighboring holes. At this midpoint, there are positive contributions to the free energy from the neighboring occupied holes. Thus a higher free energy of the pinned vortex, or $n > n_0$, would still be an equilibrium state of the system. Equation (2) should therefore be considered as a lower limit on the equilibrium number of vortices pinned to a hole. The fact that interactions should raise estimated occupation numbers was also noted in Ref. 27.

We now compare these theoretical estimates to the experimental values of $n_{\max}$. We observed three decreasing steps in T_{IL} [see Fig. 2(c)], with $\tilde{T}_6 \simeq 72\ \mathrm{K}$, $\tilde{T}_5 \simeq 75\ \mathrm{K}$, and $\tilde{T}_4 \simeq 77\ \mathrm{K}$. According to the schematic phase diagram plotted in Fig. 8(d), the values of $\tilde{T}_n$ are lower than the temperatures T_n at which the nth multiquanta vortex depins in the absence of thermal fluctuations. From the schematic description in Fig. 8(c), we see that the difference $T_n - \tilde{T}_n$ may be estimated from the difference in the T_{IL} at, and slightly away from, $B/B_\phi = n$. From Figs. 6(c) and 7(c), we estimate this difference to be $T_n - \tilde{T}_n \sim 2\ \mathrm{K}$. T_6, T_5, and T_4 are thus 74, 77, and 79 K, respectively, or, equivalently, $n_{\max}(T<74)=6$, $n_{\max}(74<T<77)=5$, $n_{\max}(77<T<79)=4$, and $n_{\max}(T>79)=3$. We find that the extracted $n_{\max}$ values are much lower than the estimated n_s and slightly higher than the estimated n_0. Thus the equilibrium multiquanta pinning scenario described by Eq. (2) is more plausible. Note, however, that Eqs. (1) and (2) are based on the assumption of fully penetrating holes; the number of vortices trapped by surface holes may be lower.[60,61]

Summarizing our discussion of the IL, the multiquanta scenario provides a more consistent explanation as compared to single-vortex pinning, both for the steps in the IL and for the similar MI fingers at both commensurate and incommensurate matching fields. Indeed, recent simulations of BSCCO with surface holes similar to those in the experiment[62] indicate that multiple-quanta occupation of surface holes does occur, and that depinning may occur directly from holes.

Finally, we address the apparent contradiction of observing a FOT within the patterned regions *at matching fields* $B/B_\phi = 1$ and 2, as shown in Figs. 6 and 7. The observed FOT occurs at the same field and temperature values as the pristine solid-liquid transition T_m, and we therefore assume that both transitions are of similar nature. This, however, seems to contradict the existence of MI phases at matching fields since in the MI phase the vortex lattice is ordered, pinned, and incompressible up to temperatures well above the pristine T_m.

The observed FOT can be understood qualitatively by taking the bulk beneath the surface holes into account. The surface holes are only $\sim 1.4\ \mu\mathrm{m}$ deep, whereas the sample is $30\ \mu\mathrm{m}$ thick. Although the depth at which vortices are still sensitive to surface patterning is not known exactly, magnetic decorations of BSCCO crystals with square Fe periodic surface patterns indicate that the hexagonal structure of the lattice is recovered fully just $4.5\ \mu\mathrm{m}$ beneath the pinning potential at low temperatures.[63] Thus one may expect that, sufficiently deep below the upper surface, the vortex "tails" will undergo a first-order melting transition at the pristine T_m. At matching fields, however, the "tips" of the vortices at the surface are pinned to the periodic surface holes and therefore behave as an incompressible solid. The resulting situation immediately above T_m is rather unique: the vortex tips are in a solid MI state, while the vortex tails are liquid. At the FOT, the vortex density in the bulk increases by $\Delta B/\phi_0$, where ΔB is the typical step in B at T_m. If the tips of the vortices were fully incompressible, this ΔB in the bulk would be completely shielded and unobservable at the top surface. Our data indicate, however, that within our experimental range of parameters the compressibility is high, but finite. Hence the MI top layer is sufficiently transparent to allow observation of the paramagnetic peak at the FOT of the underlying vortex tails. We conclude that upon increasing temperature, the FOT observed within the patterned region at matching fields indicates a transition from a solid bulk with an incompressible solid surface to a unique state of an essentially incompressible solid crust of vortex tips concealing a vortex liquid in the bulk.

It is interesting to note that this solid crust could be used as a tool to study the interesting possibility of surface melting that was suggested to exist in the vortex lattice,[40,64] similar to surface wetting in atomic solids. This will require investigating crystals of different thicknesses and samples patterned with holes at both the top and bottom surfaces.

No additional FOTs were observed, even in the presence of shaking. This indicates that the depinning line of the interstitial vortices, and the delocalization line of the vortices pinned to holes, are apparently not FOTs. More accurate magnetization measurements in the presence of shaking are needed to check for the existence of second-order thermodynamic transitions.

V. CONCLUSIONS

BSCCO crystals with arrays of surface holes were measured using differential magneto-optics accompanied by an in-plane shaking field. We observe reduced dB/dH of the patterned regions at integer matching fields $B = nB_\phi$. These features are extremely narrow, with a width in H of less than 1 Oe. The region of reduced dB/dH extends up to 87 K for the first matching field, terminating 3.5 K below T_c. Shaking allowed the equilibrium matching feature to be observed both above and below the pristine melting line of the sample. This observation is in contrast to previous dynamic measurements of BSCCO crystals with periodic surface holes,[35,38] in which matching effects were observed only well above the pristine melting line. Our finding of a sharply suppressed compressibility of an equilibrated vortex lattice at the matching fields is strong evidence of the existence of Mott insulator phases.

We observe a first-order melting transition within the patterned areas, both away from matching and at the first and second matching fields. Surprisingly, this transition is not shifted with respect to the pristine melting transition. We interpret this transition as first-order melting of the vortices in the pristine bulk beneath the patterned surface that results in a step in vortex density. The added vortex tails beneath the patterned surface force vortex tips through the surface, even in regions of reduced compressibility. We emphasize that this is an extremely unusual situation, in which the vortex tails located in the bulk are in a liquid phase, while their tips located near the surface are in a pinned, ordered phase, and therefore solid.

The irreversibility line of the patterned regions is found to be shifted upward in H and T to above the pristine melting line T_m and displays steplike behavior, with almost no temperature dependence between matching fields $B=nB_{\phi}$. These steps are consistent with a multivortex pinning scenario, with an estimated maximum value of $n_{\max}=6$ flux quanta pinned to each surface hole at $H/B_{\phi}\gtrsim 5$ and $T\leq 72$ K.

Applied shaking shifts the irreversibility line to lower field and temperature, enabling the observation of the first-order transition. However, no first-order transitions related to the surface holes, corresponding to depinning lines of interstitial vortices, or delocalization of vortices pinned to holes, were observed. Further transport measurements are necessary to determine if an additional delocalization line exists at higher temperatures, in analogy to the delocalization line of the vortices residing on columnar defects that separates the interstitial liquid from a homogeneous liquid.[12]

ACKNOWLEDGMENTS

We wish to thank A. Lahav for technical assistance. We are grateful to Y. Goldschmidt and M. Opferman for providing insights from simulations. We thank V. B. Geshkenbein, E. H. Brandt, and G. P. Mikitik for helpful discussions. This work was supported by the U.S.-Israel Binational Science Foundation (BSF), by the Minerva Foundation, and by Grant-in-aid from the Ministry of Education, Culture, Sport, Science and Technology, Japan. E.Z. acknowledges the support of the German Israeli Foundation (GIF).

[1] L. Civale, A. D. Marwick, T. K. Worthington, M. A. Kirk, J. R. Thompson, L. Krusin-Elbaum, Y. Sun, J. R. Clem, and F. Holtzberg, Phys. Rev. Lett. **67**, 648 (1991).
[2] M. Konczykowski, F. Rullier-Albenque, E. R. Yacoby, A. Shaulov, Y. Yeshurun, and P. Lejay, Phys. Rev. B **44**, 7167 (1991).
[3] D. R. Nelson and V. M. Vinokur, Phys. Rev. B **48**, 13060 (1993).
[4] G. Blatter, M. V. Feigel'man, V. B. Geshkenbein, A. I. Larkin, and V. M. Vinokur, Rev. Mod. Phys. **66**, 1125 (1994).
[5] L. Radzihovsky, Phys. Rev. Lett. **74**, 4923 (1995).
[6] A. V. Lopatin and V. M. Vinokur, Phys. Rev. Lett. **92**, 067008 (2004).
[7] S. Tyagi and Y. Y. Goldschmidt, Phys. Rev. B **67**, 214501 (2003).
[8] C. Dasgupta and O. T. Valls, Phys. Rev. Lett. **91**, 127002 (2003).
[9] C. J. van der Beek, M. Konczykowski, A. V. Samoilov, N. Chikumoto, S. Bouffard, and M. V. Feigel'man, Phys. Rev. Lett. **86**, 5136 (2001).
[10] S. S. Banerjee *et al.*, Phys. Rev. Lett. **90**, 087004 (2003).
[11] M. Menghini, Y. Fasano, F. de la Cruz, S. S. Banerjee, Y. Myasoedov, E. Zeldov, C. J. van der Beek, M. Konczykowski, and T. Tamegai, Phys. Rev. Lett. **90**, 147001 (2003).
[12] S. S. Banerjee *et al.*, Phys. Rev. Lett. **93**, 097002 (2004).
[13] A. T. Fiory, A. F. Hebard, and S. Somekh, Appl. Phys. Lett. **32**, 73 (1978).
[14] A. N. Lykov, Solid State Commun. **86**, 531 (1993).
[15] D. J. Morgan and J. B. Ketterson, Phys. Rev. Lett. **80**, 3614 (1998).
[16] V. V. Moshchalkov, M. Baert, V. V. Metlushko, E. Rosseel, M. J. Van Bael, K. Temst, Y. Bruynseraede, and R. Jonckheere, Phys. Rev. B **57**, 3615 (1998).
[17] M. Baert, V. V. Metlushko, R. Jonckheere, V. V. Moshchalkov, and Y. Bruynseraede, Phys. Rev. Lett. **74**, 3269 (1995).
[18] J. I. Martín, M. Vélez, J. Nogués, and I. K. Schuller, Phys. Rev. Lett. **79**, 1929 (1997).
[19] E. Rosseel, M. Van Bael, M. Baert, R. Jonckheere, V. V. Moshchalkov, and Y. Bruynseraede, Phys. Rev. B **53**, R2983 (1996).
[20] V. V. Metlushko, L. E. De Long, M. Baert, E. Rosseel, M. J. Van Bael, K. Temst, V. V. Moshchalkov, and Y. Bruynseraede, Europhys. Lett. **41**, 333 (1998).
[21] V. Metlushko, U. Welp, G. W. Crabtree, Z. Zhang, S. R. J. Brueck, B. Watkins, L. E. DeLong, B. Ilic, K. Chung, and P. J. Hesketh, Phys. Rev. B **59**, 603 (1999).
[22] L. E. De Long, V. V. Metlushko, S. Kryukov, M. Yun, S. Lokhre, V. V. Moshchalkov, and Y. Bruynseraede, Physica C **369**, 118 (2002).
[23] A. V. Silhanek, S. Raedts, M. J. Van Bael, and V. V. Moshchalkov, Phys. Rev. B **70**, 054515 (2004).
[24] I. B. Khalfin and B. Y. Shapiro, Physica C **207**, 359 (1993).
[25] C. Reichhardt, C. J. Olson, and F. Nori, Phys. Rev. B **57**, 7937 (1998).
[26] M. M. Doria and S. C. B. de Andrade, Phys. Rev. B **60**, 13164 (1999).
[27] G. R. Berdiyorov, M. V. Milošević, and F. M. Peeters, Phys. Rev. B **74**, 174512 (2006).
[28] M. F. Laguna, C. A. Balseiro, D. Domínguez, and F. Nori, Phys.

Rev. B **64**, 104505 (2001).
[29] C. Reichhardt, C. J. Olson, R. T. Scalettar, and G. T. Zimányi, Phys. Rev. B **64**, 144509 (2001).
[30] K. Harada, O. Kamimura, H. Kasai, T. Matsuda, A. Tonomura, and V. V. Moshchalkov, Science **274**, 1167 (1996).
[31] S. B. Field, S. S. James, J. Barentine, V. Metlushko, G. Crabtree, H. Shtrikman, B. Ilic, and S. R. J. Brueck, Phys. Rev. Lett. **88**, 067003 (2002).
[32] L. Van Look, E. Rosseel, M. J. Van Bael, K. Temst, V. V. Moshchalkov, and Y. Bruynseraede, Phys. Rev. B **60**, R6998 (1999).
[33] A. Castellanos, R. Wördenweber, G. Ockenfuss, A. v. d. Hart, and K. Keck, Appl. Phys. Lett. **71**, 962 (1997).
[34] A. Crisan, A. Pross, D. Cole, S. J. Bending, R. Wördenweber, P. Lahl, and E. H. Brandt, Phys. Rev. B **71**, 144504 (2005).
[35] S. Ooi, T. Mochiku, S. Ishii, S. Yu, and K. Hirata, Physica C **445-448**, 260 (2006).
[36] S. Ooi, T. Mochiku, M. Gaifullin, and K. Hirata, Physica C **460-462**, 1220 (2007).
[37] S. Ooi, T. Mochiku, and K. Hirata, Physica C **463-465**, 271 (2007).
[38] S. Ooi, T. Mochiku, S. Yu, E. Sadki, and K. Hirata, Physica C **426–431**, 113 (2005).
[39] E. Zeldov, D. Majer, M. Konczykowski, V. B. Geshkenbein, V. M. Vinokur, and H. Shtrikman, Nature (London) **375**, 373 (1995).
[40] A. Soibel, E. Zeldov, M. Rappaport, Y. Myasoedov, T. Tamegai, S. Ooi, M. Konczykowski, and V. B. Geshkenbein, Nature (London) **406**, 282 (2000).
[41] M. Tokunaga, M. Kobayashi, Y. Tokunaga, and T. Tamegai, Phys. Rev. B **66**, 060507(R) (2002).
[42] N. Avraham, E. H. Brandt, G. P. Mikitik, Y. Myasoedov, M. Rappaport, E. Zeldov, C. J. van der Beek, M. Konczykowski, and T. Tamegai, Phys. Rev. B **77**, 214525 (2008).
[43] M. Willemin, A. Schilling, H. Keller, C. Rossel, J. Hofer, U. Welp, W. K. Kwok, R. J. Olsson, and G. W. Crabtree, Phys. Rev. Lett. **81**, 4236 (1998).
[44] B. Schmidt, M. Konczykowski, N. Morozov, and E. Zeldov, Phys. Rev. B **55**, R8705 (1997).
[45] N. Morozov, E. Zeldov, D. Majer, and M. Konczykowski, Phys. Rev. B **54**, R3784 (1996).
[46] C. Wengel and U. C. Täuber, Phys. Rev. B **58**, 6565 (1998).
[47] D. Majer, E. Zeldov, and M. Konczykowski, Phys. Rev. Lett. **75**, 1166 (1995).
[48] N. Avraham *et al.*, Nature (London) **411**, 451 (2001).
[49] H. Beidenkopf, N. Avraham, Y. Myasoedov, H. Shtrikman, E. Zeldov, B. Rosenstein, E. H. Brandt, and T. Tamegai, Phys. Rev. Lett. **95**, 257004 (2005).
[50] H. Beidenkopf, T. Verdene, Y. Myasoedov, H. Shtrikman, E. Zeldov, B. Rosenstein, D. Li, and T. Tamegai, Phys. Rev. Lett. **98**, 167004 (2007).
[51] N. Morozov, E. Zeldov, D. Majer, and B. Khaykovich, Phys. Rev. Lett. **76**, 138 (1996).
[52] T. Schuster, M. V. Indenbom, H. Kuhn, E. H. Brandt, and M. Konczykowski, Phys. Rev. Lett. **73**, 1424 (1994).
[53] E. Zeldov, A. I. Larkin, V. B. Geshkenbein, M. Konczykowski, D. Majer, B. Khaykovich, V. M. Vinokur, and H. Shtrikman, Phys. Rev. Lett. **73**, 1428 (1994).
[54] N. Morozov, E. Zeldov, M. Konczykowski, and R. A. Doyle, Physica C **291**, 113 (1997).
[55] O. M. Stoll, M. I. Montero, J. Guimpel, J. J. Åkerman, and I. K. Schuller, Phys. Rev. B **65**, 104518 (2002).
[56] G. S. Mkrtchyan and V. V. Schmidt, Sov. Phys. JETP **34**, 195 (1972).
[57] C. Wengel and U. C. Täuber, Phys. Rev. Lett. **78**, 4845 (1997).
[58] A. I. Buzdin, Phys. Rev. B **47**, 11416 (1993).
[59] T. Jacobs, S. Sridhar, Q. Li, G. D. Gu, and N. Koshizuka, Phys. Rev. Lett. **75**, 4516 (1995).
[60] A. Bezryadin, Y. N. Ovchinnikov, and B. Pannetier, Phys. Rev. B **53**, 8553 (1996).
[61] S. Raedts, A. V. Silhanek, M. J. Van Bael, and V. V. Moshchalkov, Phys. Rev. B **70**, 024509 (2004).
[62] Y. Y. Goldschmidt and M. Opferman (unpublished).
[63] Y. Fasano, M. Menghini, and F. de la Cruz, Physica C **408-410**, 474 (2004).
[64] A. DeCol, G. I. Menon, V. B. Geshkenbein, and G. Blatter, Phys. Rev. Lett. **96**, 177001 (2006).